# 1. Study on MOVPE growth of III-Nitrides Heteroepitaxial films and their application to electronic devices

# Chapter 1

# Introduction

## 1.1. Foreword

The remarkable advance of solid-state electronics in the 20th century has largely contributed to the establishment of today's highly-networked information society, and in recent years, the demand for solid-state electronic devices has been continually increasing with the development of wireless communications, telecommunications, data communications and aerospace systems. The requirements include aspects of high power level, high efficiency, high linearity and high operating frequency. One major trend is the continuous demand for higher power at higher frequencies. Si- and GaAs-based power devices have been very reliable workhorses at high frequencies especially microwave spectrum. However, their power performances have already been pushed close to their theoretical limit. Under such circumstance, wide bandgap semiconductors with an order of magnitude or so higher breakdown voltage along with excellent thermal properties began to emerge. For many years, SiC has been widely touted as a potential candidate, but unfortunately it does not appear to be a truly microwave technology in terms of its relatively low carrier mobility. With technological and cost advantages over competing SiC, GaN and related III-nitrides semiconductor materials has quickly gained the center attention. In terms of electronic material properties, GaN possessed very attractive features such as large bandgap (3.4 eV), high breakdown field ($> 3 \times 10^6$ V/cm), the existence of modulation doped AlGaN/GaN structures with attendant high

electron mobility (≥ 1200 $cm^2/Vs$) and extremely high peak ($3 \times 10^7$ cm/s) and saturation electron velocity ($2 \times 10^7$ cm/s). Also GaN has been successfully grown on sapphire or SiC substrates. Therefore, GaN-based electronic devices have recently been attracting much attention for the realization of high-power and high-frequency electronic devices.

## 1.2. Features of GaN and related III-nitrides and their applications

GaN and related III-nitrides semiconductor materials have been viewed as highly promising for optoelectronic device applications at blue and ultraviolet (UV) wavelengths [1-8] in much the same manner that its highly successful As- and P-based counterparts have been

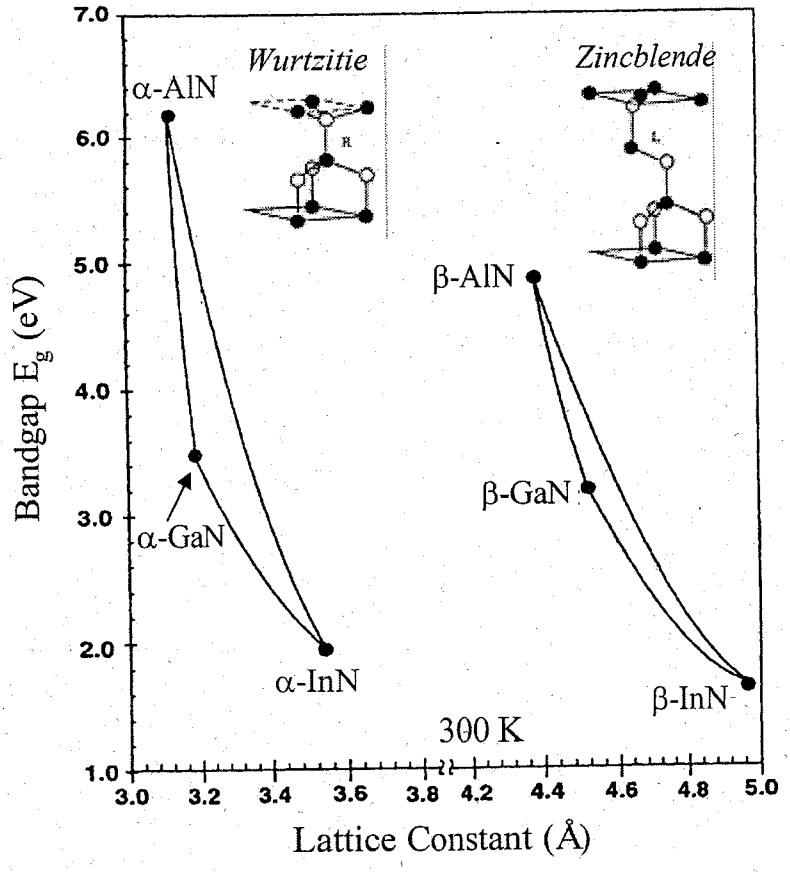


FIG. 1.1. Bandgap of Wurtzite and Zincblende type InN, GaN, and AlN and their alloys versus lattice constant *a*.

exploited for infrared, red and yellow wavelength. III-nitrides systems such as AlN, GaN, InN and their alloys are all wide-bandgap semiconductor materials, and they can be crystallized in Wurtzite and Zincblende polytypes. Wurtzite GaN, AlN and InN have direct bandgaps of 3.4 eV, 6.2 eV and 0.7-1.9 eV at room temperature, respectively (see Figure 1.1). In view of the available wide range of direct bandgaps, GaN alloyed with AlN and InN may span a continuous range of direct bandgap energies throughout much of the visible spectrum well into the UV wavelengths. This makes the nitride system attractive for optoelectronic device applications, such as light emitting diodes (LEDs) [1-7], laser diodes (LDs) [8], and photo detectors, which are active in the green, blue or UV wavelengths.

Another area gaining a lot of attention for III-nitrides is high temperature and high power electronics. The interest stems from some intrinsic properties of this group of semiconductors. The first is their wide bandgap nature. The wide bandgap materials such as GaN and SiC are promising for high temperature applications because they go intrinsic at much higher temperatures than other traditional semiconductor materials such as Ge, Si and GaAs. It means that GaN power devices can operate with less cooling and fewer high cost processing steps associated with complicated structures designed to maximize heat extraction. The second attractive property of III-nitrides is that they have high breakdown fields. The critical electric field of the breakdown scales roughly with the square of the energy bandgap, and has been estimated to be as high as 3.3 MV/cm for GaN compared with 0.3 and 0.4 MV/cm for Si and GaAs, respectively [9]. Figure 1.2 is a plot of avalanche and punch through breakdown of GaN Schottky diodes calculated as a function of doping concentration and standoff layer thickness. It can be seen that 20 kV devices may be obtained with a 100 μm thick GaN layer with a doping concentration $< 10^{15}$ $cm^{-3}$.

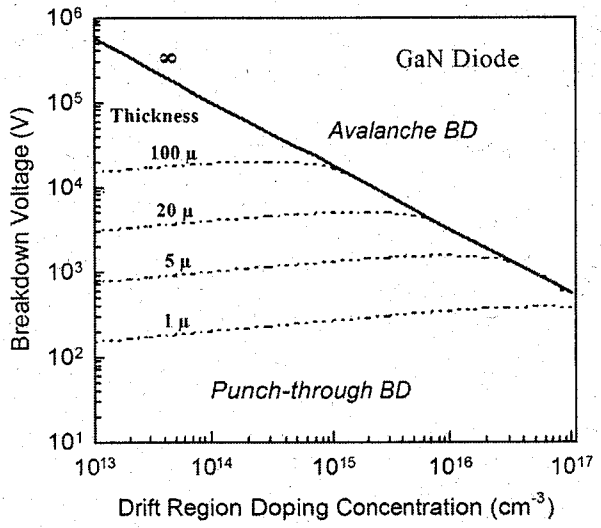


FIG. 1.2. Calculated breakdown voltage as a function of doping concentration and thickness of the drift region in GaN Schottky diodes.

GaN has also excellent electron transport properties, including good mobility and high saturated drift velocity as shown in Figure 1.3 [10]. This makes it adequate for general electronics, and promising for microwave rectifiers, particularly. The material properties associated with high temperature, high power, and high frequency applications of GaN and several conventional semiconductors are summarized in Table 1.1 [11-14]. It is anticipated that GaN may eventually prove to be superior to SiC in this area.

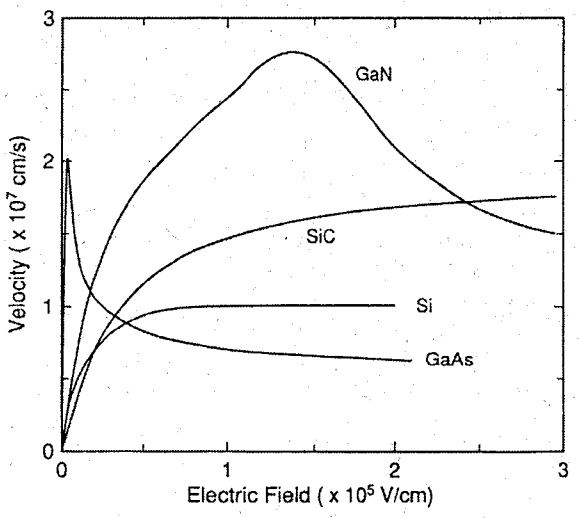


FIG. 1.3. Electron drift velocity at 300 K in GaN, SiC, Si and GaAs computed using the Monte Carlo technique.

TABLE 1.1. Comparison of material properties in various semiconductors at 300K. (CFOM = Combined Figure of Merit for high temperature/high power/high frequency applications)

| Property | Si | GaAs | 6H-SiC | 4H-SiC | GaN |
|---|---|---|---|---|---|
| Bandgap $Eg$ (eV) | 1.12 | 1.43 | 2.86 | 3.02 | 3.39 |
| Breakdown Field $E_B$ (MV/cm) | 0.3 | 0.4 | 3.0 | 3.0 | 3.0 |
| Electron Mobility $\mu$ ($cm^2$/Vs) | 1500 | 8500 | 800 | 460 | 2000 |
| Maximum Velocity $v_s$ ($10^7$ cm/s) | 1.0 | 2.0 | 2.0 | 2.7 | 2.7 |
| Thermal Conductivity $\chi$ (W/cmK) | 1.5 | 0.5 | 4.9 | 4.9 | 1.5 |
| Dielectric Constant $\varepsilon$ | 11.8 | 12.8 | 10 | 9.7 | 9.5 |
| CFOM = $\chi\varepsilon\mu v_s E_B^2/(\chi\varepsilon\mu v_s E_B^2)_{Si}$ | 1 | 7 | 295 | 222 | 290 |

The most attractive feature of III-nitrides compared with SiC is the heterostructure technology. Quantum well, modulation-doped heterointerface, and heterojunction structures can all be formed in this system and give access to new spectral regions for optical devices and new operation regimes for electronic devices. Figure 1.4 schematically shows a conduction-band diagram of AlGaN/GaN heterostructures. Due to the large conduction-band discontinuity, electrons diffusing from the larger-bandgap AlGaN into the smaller-bandgap GaN form a two-dimensional electron gas (2DEG) in the triangle quantum-well at the AlGaN/GaN heterointerface. Furthermore, the sheet carrier density of the 2DEG is enhanced by strong piezoelectric effects in GaN and AlGaN. Piezoelectric coefficients of Wurtzite-type III-nitrides are approximately one order of magnitude higher than those of traditional III-V material such as GaAs and InP [15].

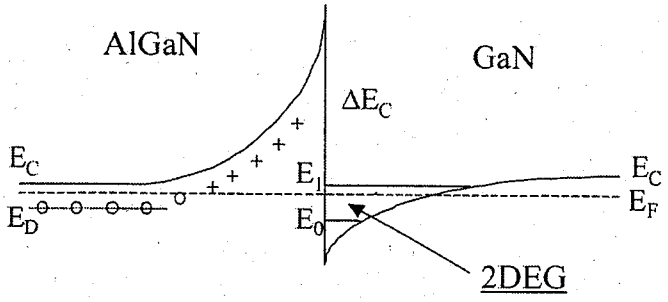


FIG. 1.4. Schematic drawing of conduction band structure in an AlGaN/GaN structure.

## 1.3. Recent progress in GaN-based electronic devices

The nitride material growth technology that supports the optical device efforts has also proven to be compatible with the development of electronic devices. In the past decade, the development of GaN-based electronic devices has emphasized field effect transistor (FET) structures, especially in high-electron-mobility transistors (HEMTs), because this important class of devices put smaller demands on the growth and fabrication technique compared with other electronic devices. HEMTs are FETs that use a band-offset between similar semiconductor materials to create a 2DEG. The 2DEG forms an excess of charge carriers on one side of the material interface, and they acts analogously to the channel in standard FETs. HEMTs are also known as HFETs, HJFETs, and many other names, which tend to indicate specific characteristics of the device. The 2DEG may be formed because of polarity effects in the material in undoped-polar semiconductors or because of the doping in any semiconductor. In general, 2DEG mobility and density determine the performance of HEMTs.

AlGaN/GaN heterostructures have much higher 2DEG densities than in similar AlGaAs/GaAs heterostructures due to their large conduction-band discontinuity and strong piezoelectric effects, as presented in section 1.2. In addition, theoretical simulations have predicted a high peak electron velocity of ~$3 \times 10^7$ cm/s and an electron mobility of ~2000 $cm^2/Vs$ in the GaN channel at room temperature [16,17]. Thus HEMTs based on AlGaN/GaN heterostructures have been very promising research subjects for the realization of high-power electronic devices for high frequency operations. The recent progress in these devices has been sufficient to show that GaN and related alloys will play a significant role in the future development of high-power and high-frequency electronic devices. In 1993, Khan *et al.* demonstrated the first AlGaN/GaN HEMT, with an extrinsic transconductance $g_m$ of 23 mS/mm and 2DEG mobility of 563 $cm^2/Vs$ at 300 K [18]. They also reported the first microwave

results with a cut-off frequency ($f_T$) of 11 GHz and a maximum oscillation frequency ($f_{max}$) of 14 GHz [19]. In the past decade, with rapid progress in the growth and process technology, the transconductance, operating frequency, current capacity and breakdown voltage are all increased to the point that GaN-based HEMTs are now strong contenders in the arena of high-power and high-frequency applications. To date, a total output power of 250 W at 2.1 GHz is reported for a GaN-based power amplifier, which was designed for the application in W-CDMA base stations [20]. The highest $g_m$ of 450 mS/mm is achieved for a 0.15-μm-gate-length HEMT grown on a SiC substrate [21], and the highest $f_T$ and $f_{max}$ of 152 GHz and 173 GHz are also reported for a 60-nm-gate-length AlGaN/GaN HEMT grown by plasma-assisted molecular-beam epitaxy (PAMBE) [22]. The remarkable performance of GaN-based HEMTs has also been demonstrated in applications to high-speed switching ICs [23] or high-power DC-DC converters [24]. A high breakdown voltage of 1.3 kV is achieved for an insulating-gate structure GaN HEMT [25]. A high current handling capability of 150 A with an off-state breakdown voltage of 350 V is reported for a 5.6 mm × 2.8 mm HEMT die with a source-via grounding structure [26].

One of the main themes in current researches on GaN-based HEMTs is the improvement of their 2DEG properties. Different growth methods, different substrates and novel structures have been tried to achieve large 2DEG densities and high mobilities [27-34]. Recently, modified AlGaN/AlN/GaN structures [27,28], which employ a thin AlN interfacial layer between the AlGaN and GaN layers, showed very interesting properties in terms of enhancing the 2DEG properties [27,28]. Most noteworthy is an AlGaN/AlN/GaN HEMT with a 1-nm-thick AlN layer grown on a SiC substrate, which showed a room-temperature Hall mobility of 1540 $cm^2/Vs$ with a 2DEG density of $1.48 \times 10^{13}/cm^2$ [28]. This is reported to be because of the reduction of the alloy disorder scattering due to the suppression of the carrier penetration from the GaN channel into the AlGaN layer [27,28,35].

## 1.4. GaN growth technology: current status and issues

Substantial research on III-nitrides growth was initiated in early 1960s. However, they have trailed way behind the easier-to-grow Si and GaAs semiconductors on the development curve. Nearly 30 years later, Si and GaAs have been pushed to their theoretical limits, while nitrides are just beginning to show their promise. The technological spin-offs came late because ideal substrates could not be found and consequently GaN films contained substantial concentration of defects and had high n-type background.

One particular difficulty in the growth of GaN is the unavailability of sufficiently large (> 1 cm) single crystals for use as substrates for homoepitaxial growth. Thus, up to now, heteroepitaxial growth has been a practical necessity and the choice of substrate has been critical. Possible substrate materials should have low thermal expansion and lattice mismatch with the grown crystals. Also, they should be unaffected by the growth chemistries such as $NH_3$ or $H_2$ at high growth temperatures (in excess of 1000°C in some cases). Under these constraints, sapphire ($Al_2O_3$) and SiC are the most popular substrate materials used currently. When hexagonal GaN is grown on the (0001) basal plane of sapphire, a lattice misfit of ~13% at the growth temperatures can generate dense dislocations and defects in the thin film. In the practical case, a large part of the misfit is relaxed through three-dimensional (3D) island growth. The residual strain in the thin film is comparable to the lattice misfit between GaN and substrate material, and the result is comparable to the dislocation densities observed. The ideal candidate substrate is clearly a GaN wafer. Several research groups are investigating the growth of the bulk GaN crystals and very thick films through various techniques [36-39]. However, commercially available GaN wafers with sufficiently large-area and high-quality crystals appear to be several years away. The nitride community will continuously be challenged with heteroepitaxial growth in the foreseeable future.

Metalorganic vapor phase epitaxy (MOVPE) has evolved into a leading technique for production of III-nitrides devices. One remarkable application worthy to be mentioned is the achievement of super-bright blue LEDs [5]. Initially the growth of GaN was performed directly on sapphire or SiC substrates. However, the wafer usually had large crystalline defects with rough surfaces mainly caused by the 3D growth mode. In 1986, Amano *et al.* [40] succeeded in remarkably improving the GaN surface morphology as well as the electrical and optical properties by deposition of a thin low-temperature buffer layer (LT-BL) prior to the high temperature growth of GaN. This also lowered the large background electron concentrations from previous $10^{19}$–$10^{20}/cm^3$ levels to $10^{17}/cm^3$, which not only improved the crystal quality but also set the stage for p-type doping [1].

The essential role of LT-BLs is both to supply nucleation and promote lateral growth of the GaN film due to the decrease in interfacial free energy between the film and the substrate. However, although the LT-BL technique has reduced the effects of the lattice mismatch, the defect densities in these films are still on the order of one million times higher than in other semiconductor systems. These defect-laden materials, to date, have had a surprisingly small effect on the performance of both optical and electronic devices, but they may raise major questions as to the long-term stability of these devices. It is unlikely that the full promise of GaN and related alloys can be realized without a major reduction in the defect densities in the as-grown materials.

Up to now, many investigations for the GaN growth have been reported on small-area 50-mm-diameter substrates. To consider the mass production of electronic devices, however, large-area wafers ($\geq$ 100 mm in diameter) would extremely be indispensable because they can be readily applied to existing device manufacturing lines based on Si and/or GaAs-related technology. Thus, the development of large-area epiwafers, which requires the development of the growth technology as well as the underlying substrates, is now strongly required.

## 1.5. Scope and purpose of dissertation

Recent progress in the growth technology of GaN and related alloys has led to the demonstration of very impressive results in devices for high-power and high-frequency applications. However, there are still some issues to be solved in order to consider the practical application of nitride-HEMTs.

The first is the development of growth technologies on large-area substrates. For the present, many investigations for GaN-based HEMTs have been reported only on 50-mm-diameter substrates. For the mass production of electronic devices such as HEMTs, however, the development of growth technologies using substrates larger than 100 mm in diameter is strongly required. For epitaxial growth on large-area substrates, it is difficult to realize good uniformity of crystal quality, alloy composition and 2DEG properties across the entire epitaxial wafer.

The second is the development of high-crystal quality epitaxial films with high-quality 2DEG properties. Although the LT-BL technique has reduced the effects of the lattice mismatch, the defect densities in MOVPE-grown GaN films are still high compared with other semiconductor systems. These defect-laden materials may raise major questions as to the long-term stability of these devices. High-crystal-quality epitaxial films with high 2DEG properties are now required in order to obtain reliable devices.

We believe that we can contribute to the manufacturing of GaN HEMTs by developing large-area and high-quality epitaxial wafers. This dissertation has focused on the MOVPE growth of high-quality and high-performance GaN HEMTs on large-area substrates. All the work is directed towards the development and understanding of the MOVPE-growth technology for GaN HEMTs. In order to examine the practical application of GaN HEMT epiwafers, it is also important to understand their basic structural and electrical properties as well as their basic

device characteristics. Therefore, HEMTs were fabricated using MOVPE-grown epitaxial wafers, point by point, and their device performance was characterized. Also, to understand the basic electrical properties in MOVPE-grown epitaxial films, 2DEG transport properties were theoretically studied in detail.

Chapter 2 reports the growth technology for uniform growth of different-Al-content AlGaN/GaN HEMT structures with the highest Al content of 70 mol% on 100-mm-diameter sapphire substrates. HEMTs were fabricated on those wafers and characterized. The uniformity study of DC characteristics in HEMTs was also performed on a 100-mm-diameter epitaxial wafer.

Chapter 3 discusses the structural and 2DEG transport properties in MOVPE-grown AlGaN/GaN HEMT structures. The dominant 2DEG scattering processes in AlGaN/GaN HEMT structures are investigated in detail.

Chapter 4 deals with modified AlGaN/AlN/GaN HEMT structures including a thin AlN interfacial layer, which are reported to show higher 2DEG properties than those in conventional AlGaN/GaN structures. In order to examine the possibility of MOVPE-grown AlGaN/AlN/GaN structures, their structural and electron transport properties are discussed, and HEMTs were fabricated and characterized.

Chapter 5 presents the investigation results for the growth of high-quality GaN HEMT structures. High-crystal-quality epitaxial AlN/sapphire templates, which were developed in our research group, were used as underlying substrates for achieving high-crystal-quality GaN HEMT epilayers. HEMTs were fabricated using those epiwafers. The correlation of the crystal qualities and electrical properties of HEMTs are also discussed.

Chapter 6 offers conclusions of this dissertation.

### 1.5.1. GaN MOVPE system for 100-mm-diameter substrates

In order to investigate the MOVPE-growth for GaN-based HEMT structures on 100-mm-diameter substrates, we used a large-scaled horizontal MOVPE system (Taiyo Nippon Sanso, SR-4000). Figure 1.5 shows photographs of the SR-4000 MOVPE system. This system is an enlarged version of SR-2000 (Taiyo Nippon Sanso), which is a single-wafer-charged type MOVPE system for 50-mm-diameter substrates [41]. Figures 1.6 and 1.7 show schematic drawings of the reactor in the SR-4000 system. As seen in Figure 1.7, SR-4000 has a laminar three-flow reactor. The flow liner made of quartz glass is installed in the stainless-steel chamber. A thin restricted-gas-flow liner is adopted in order to suppress thermal convection, which may cause the reduction of growth rate, uniformity, and film quality. In order to suppress undesirable gases reactions, the shape of the flow linear was carefully designed to achieve high-velocity gas flow. In this MOVPE system, $NH_3$ and its carrier gas, a mixture of group III element organometallics and their carrier gas, and the top-flow inert gas are separately injected, as seen in Figure 1.7. The upstream region of the flow liner has a three-stage structure and at this region gases injected from the three nozzles are formed into laminar flows. Diffusion of the organometallics starts at the edge of the isolation plate and growth starts at a downstream region of the reactor. In this flow liner, the concentration of organometallics near the substrate gradually increases along the stream. Growth rate, alloy composition, dopant concentration and uniformity are affected not only by the total gas flow of the three injected gases but also by the flow balance between the three injected gases [42-44]. The wafer is heated by a carbon resistance heater up to 1200°C. Trimethylgallium (TMG), Trimethylaluminum (TMA) and ammonia ($NH_3$) were used as Ga, Al and N sources, respectively, and monosilane ($SiH_4$) was used as the n-type dopant.

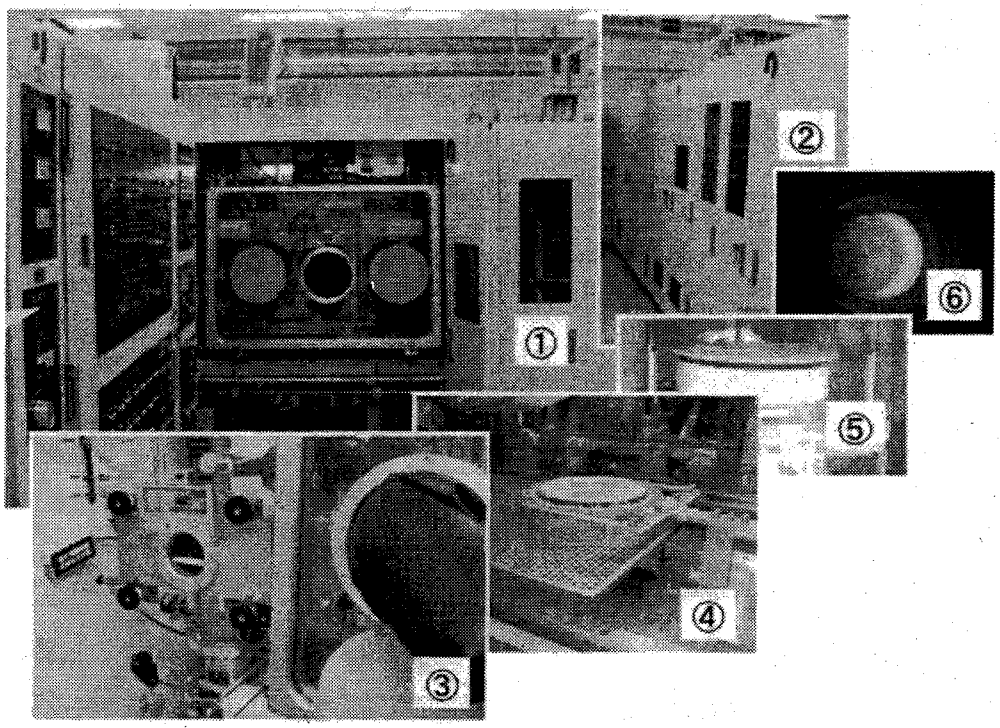


FIG. 1.5. SR-4000 GaN MOVPE system (Taiyo Nippon Sanso).

(1) front view of SR-4000, (2) reactor body, (3) pass box, (4) wafer tray in the globe box
(5) heating unit, (6) top viw of the reactor

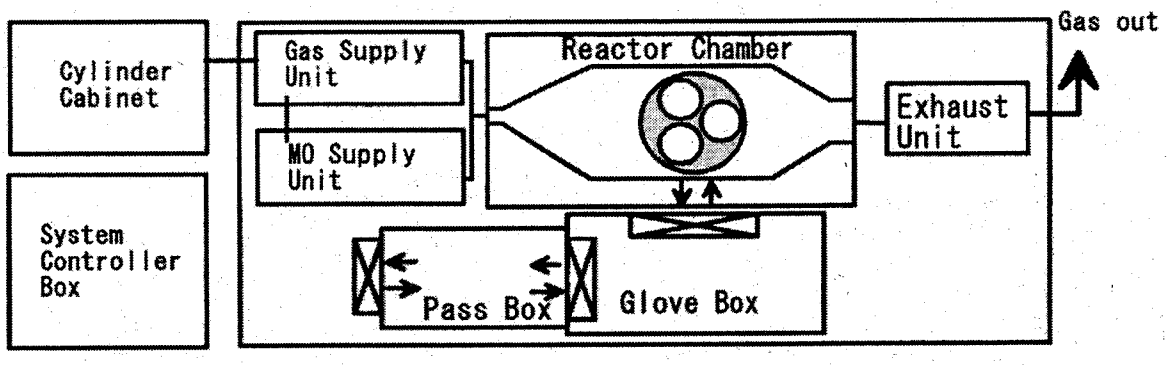


FIG. 1.6. Schematic drawing of SR-4000 GaN MOVPE system.

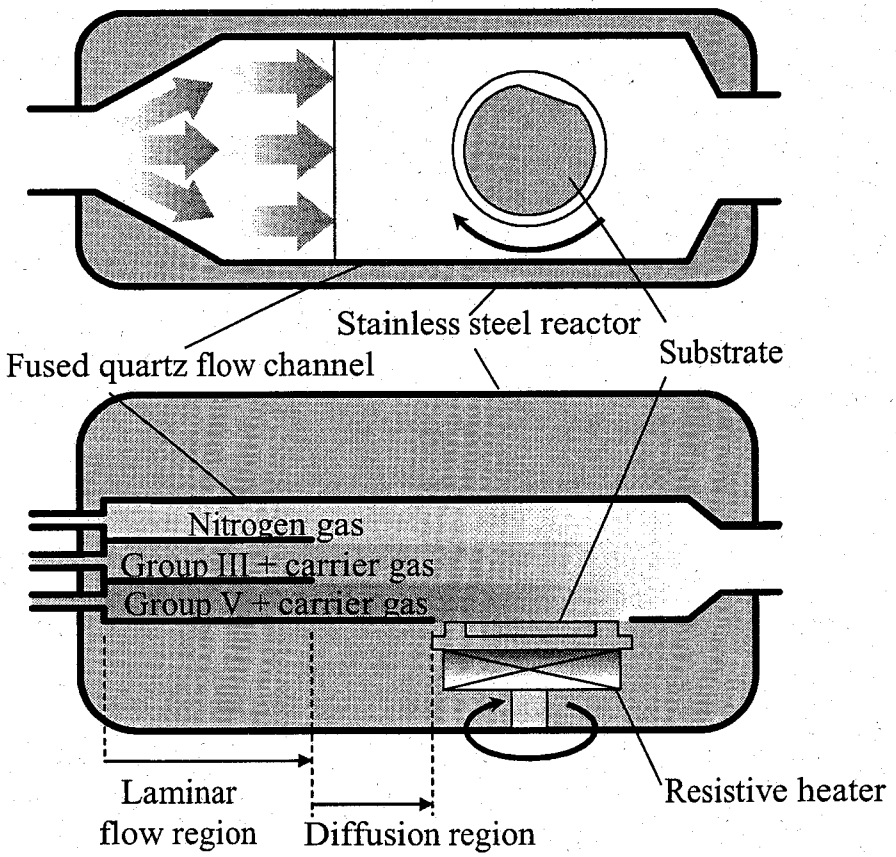


FIG. 1.7. Schematic drawing of the reactor structure in SR-4000 GaN MOVPE system.

## References


[1] H. Amano, M. Kito, K. Hiramatsu, and I. Akasaki, Jpn. J. Appl. Phys. **28**, L2112 (1989).

[2] I. Akasaki, H. Amano, M. Kito, and K. Hiramatsu, J. Lumin. **48/49**, 666 (1991).

[3] S. Nakamura, T. Mukai, and M. Senoh, Jpn. J. Appl. Phys. **30**, L1998 (1991).

[4] S. Nakamura, T. Mukai, and M. Senoh, Appl. Phys. Lett. **62**, 2390 (1993).

[5] S. Nakamura, T. Mukai, and M. Senoh, Appl. Phys. Lett. **64**, 1687 (1994).

[6] B. Goldenberg, J. D. Zook, and R. Umler, Appl. Phys. Lett. **62**, 381 (1993).

[7] R. J. Molnar, R. Singh, and T. D. Moustakas, Appl. Phys. Lett. **66**, 2390 (1995).

[8] S. Nakamura, M. Senoh, S. Nagahama, N. Iwasa, T. Yamada, T. Matsushita, H. Kiyoku, and Y. Sugimoto, Jpn. J. Appl. Phys. **35**, L74 (1996).

[9] D. K. Gaskill, C. D. Brandt, and R. J. Nemanich, *Material Research Society Symposium (MRS) Proceedings,* Pittsburgh, PA. **423**, 69 (1996).

[10] N. S. Mansour, K. W. Kim, and M. A. Littlejohn, J. Appl. Phys., **77**, 2834 (1955).

[11] H. Morkoç, S. Strite, G. B. Gao, M. E. Lin, B. Sverdlov, and M. Burns, J. Appl. Phys. **76**, 1363 (1994).

[12] T. P. Chow and R. Tyagi, IEEE Trans. Electron Devices **41**, 1481 (1994).

[13] Z. Z. Bandić, P. M. Bridger, E. C. Piquette, T. C. McGill, R. P. Vaudo, V. M. Ohanse, and J. M. Redwing, Appl. Phys. Lett. **74**, 1266 (1998).

[14] R. Gaska, J. W. Yang, A. Osinsky, Q. Chen, M. A. Khan, A. O. Orlov, G. L. Snider, and M. S. Shur, Appl. Phys. Lett. **72**, 707 (1998).

[15] P. M. Asbeck, E. T. Yu, S. S. Lau, G. J. Sulliran, J. M. Van Hove, and J. Redwing, Electron. Lett. **33**, 1230 (1997).

[16] J. D. Albrecht, R. P. Wang, P .P. Ruden, M. Farahmand, and K. F. Brennan, J. Appl. Phys.

**83**, 4777 (1998).

[17] B. E. Foutz, L. F. Eastman, U. V. Bhapkar, and M. S. Shur, Appl. Phys. Lett. **70**, 2849 (1997).

[18] M. Kahn, A. R. Bhattarai, J. N. Kuznia, D. T. Olson, Appl. Phys. Lett. **63**, 1214 (1993).

[19] M. Kahn, J. N. Kuznia, D. T. Olson, W. Schatt, J. Burn, and M. S. Shur, Appl. Phys. Lett. **65**, 1121 (1994).

[20] T. Kikkawa, T, Maniwa, H. Hayashi, M. Kanamura, S. Yokokawa, M. Nishi, N. Adachi, M. Yokoyama, Y. Tateno, and K. Johshin, *Tech. Digest in the IEEE Int. Microwave Symp. (IMS)*, 1347 (2004).

[21] H. Okita, K. Kaifu, J. Mita, T. Yamada, Y. Sano, H. Ishikawa, T. Egawa, and T. Jimbo, Phys. Stat. Sol. (a) **200**, 187 (2003).

[22] M. Higashiwaki and T. Matsui, Jpn. J. Appl. Phys. **44**, L475 (2005).

[23] H. Ishida, Y. Hirose, T. Murata, A. Kanda, Y. Ikeda, T. Matsuno, K. Inoue, Y. Uemoto, T. Tanaka, and D. Ueda, *Tech. Digest in the IEEE International Electron Devices Meeting (IEDM)*, 583 (2003).

[24] W. Saito, Y. Takada, M. Kuraguchi, K. Tsuda, I. Ohmura, and T. Ogura, *Tech. Digest in the IEEE International Electron Devices Meeting (IEDM)*, 587 (2003).

[25] N.-Q. Zhang, B. Moran, S. P. DenBaars, U. K. Mishra, X. W. Wang, and T. P. Ma, *Tech. Digest in the IEEE International Electron Devices Meeting (IEDM)*, 589 (2001).

[26] M. Hikita, M. Yanagihara, K. Nakazawa, H. Ueno, Y. Hirose, T. Ueda, Y. Uemoto, T. Tanaka, D. Ueda, and T. Egawa, *Tech. Digest in the IEEE International Electron Devices Meeting (IEDM)*, 803 (2004).

[27] I. P. Smorchkova, L. Chen, T. Mates, L. Shen and S. Heikman, B. Moran, S. Keller, S. P. DenBaars, J. S. Speck, and U. K. Mishra, J. Appl. Phys. **90**, 5196 (2001).

[28] L. Shen, S. Heikman, B. Moran, R. Coffie, N. -Q. Zhang, D. Buttari, I. P. Smorchkova, S.

Keller, S. P. DenBaars, and U. K. Mishra, IEEE Electron Devices Lett. **22**, 457 (2001).

[29] N. Maeda, T. Tawara, T. Saitoh, K. Tsubaki, and N. Kobayashi, Phys. Stat. Sol. (a) **200**, 168 (2003).

[30] C. X. Wang, K. Tsubaki, N. Kobayashi, T. Makimoto, and N. Maeda, Appl. Phys. Lett. **84**, 2313 (2004).

[31] I. P. Smorchkova, C. R. Elsass, J. P. Ibbetson, R. Vetury, B. Heying, P. Fini, E. Haus, S. P. DenBaars, J. S. Speck, and U. K. Mishra, J. Appl. Phys. **86**, 4520 (1999).

[32] R. Gaska, M. S. Shur, A. D. Bykhovski, A. O. Orlov, and G. L. Snider, Appl. Phys. Lett. **74**, 287 (1999).

[33] G. Y. Xhao, H. Ishikawa, T. Egawa, T. Jimbo, and M. Umeno, Jpn. J. Appl. Phys. **39**, 1035 (2000).

[34] S. Arulkumaran, M. Sakai, T. Egawa, H. Ishikawa, T. Jimbo, T. Shibata, K. Asai, S. Sumiya, Y. Kuraoka, M. Tanaka, and O. Oda, Appl. Phys. Lett. **81**, 1131 (2002).

[35] L. Hsu and W. Walukiewicz, J. Appl. Phys. **89**, 1783 (2001).

[36] V. A. Sukhoveyev, V. A. Ivantsov, I. P. Nikitina, A. I. Babanin, A. Y. Polyakov, A. V. Govorkov, N. B. Smirnov, M .G. Mil'vidskii, and V. Dmitriev, MRS Internet J. Nitride Semicond. Res. **5S1**, W6.6 (2000).

[37] A. Castaldini, A. Cavallini, L. Polenta, C. Díaz-Guerra, and J. Piqueras, J. Phys.: Condens. Matter. **14**, 13095 (2002).

[38] W. Götz, L. T. Romano, J. Walker, N. M. Johnson, and R. J. Molnar, Appl. Phys. Lett. **72**, 1214 (1998).

[39] C. Wetzel, D. Volm, B. K. Mayer, K. Pressel, S. Nilsson, E. N. Mokhov, and P. G. Baranov, Appl. Phys. Lett. **65**, 1033 (1994).

[40] H. Amano, N. Sawaki, I. Akasaki, and Y. Toyoda, Appl. Phys. Lett. **48**, 353 (1986).

[41] H. Tokunaga, I. Waki, A. Yamaguch, N. Akutsu, K. Matsumoto, J. Cryst. Growth **189/190**,

519 (1998).

[42] N. Akutsu, H. Tokunaga, K. Uchida, K. Matsumoto, *Proc. 15th Symp. on Materials Science and Engineering Research Center of Ion Beam Technology*, 77 (1996).

[43] T. Arai, J. Hidaka, H. Tokunaga, K. Matsumoto, J. Cryst. Growth **170**, 88 (1997).

[44] K. Uchida, H. Tokunaga, Y. Inaishi, N. Akutsu, K. Matsumoto, Mater. Res. Soc. Symp. Proc. **449**, 129 (1997).

# Chapter 2

# Growth of 100-mm-diameter AlGaN/GaN HEMT structures on sapphire substrates by MOVPE

## 2.1. Introduction

HEMTs based on AlGaN/GaN heterostructures are very promising electronic devices for high-power and high-frequency applications, as presented in Chapter 1. The sheet carrier density of the 2DEG generated at the AlGaN/GaN heterointerface is several times larger than that of similar AlGaAs/GaAs HEMT structures. The very high 2DEG density of AlGaN/GaN heterostructures is due to their high piezoelectric polarization [1-4] and high spontaneous polarization [4,5] around the AlGaN/GaN heterointerface. Furthermore, it has been confirmed theoretically [5-7] as well as experimentally [8-10] that the 2DEG density of AlGaN/GaN heterostructures increases with the increase in the Al content in AlGaN layers. Therefore, in order to achieve higher power densities for AlGaN/GaN HEMTs, it is effective to grow AlGaN/GaN heterostructures with higher Al contents. High-power-density HEMTs have actually been reported based on high-Al-content AlGaN/GaN heterostructures. Mishra and Wu have reported a maximum extrinsic transconductance ($g_m$) of 240 mS/mm with a maximum source-to-drain current density ($I_{DS}$) of 1130 mA/mm for 0.25-μm-gate-length $Al_{0.5}Ga_{0.5}N$/GaN HEMTs [11]. A maximum $g_m$ of 255 mS/mm and cw power densities of 2.84 W/mm and 2.57 W/mm at 8 GHz and 10 GHz, respectively, have also been reported for 0.7-μm-gate-length $Al_{0.5}Ga_{0.5}N$/GaN HEMTs [11,12].

Recently, rapid progress in MOVPE technology has enabled the fabrication of GaN-based

devices such as LEDs. Many of these investigations have, however, been reported only on 50-mm-diameter sapphire or SiC substrates. For the mass production of electronic devices including HEMTs, the development of a growth technology using substrates larger than 100 mm in diameter is necessary because such large-area wafers can be readily applied to conventional device manufacturing lines based on GaAs-related technology. Regarding higher-Al-content AlGaN/GaN heterostructures, in particular, no attempts have ever been made to grow them on practical large-area substrates. In the growth of AlGaN/GaN heterostructures by MOVPE, the gas phase reaction between Trimethylaluminum (TMA) and ammonia ($NH_3$) causes the local variation in the Al content in AlGaN layers [13,14]. For the growth of higher-Al-content AlGaN layers on large-area substrates, it is more difficult to realize good in-wafer uniformity of the Al content in AlGaN layers. This chapter reports the study on the growth of high-Al-content AlGaN/GaN HEMT structures with the highest Al content of 70 mol% on 100-mm-diameter sapphire substrates by MOVPE. HEMTs were fabricated on those HEMT epiwafers, and the device performance was characterized. The uniformity study of DC characteristics in HEMTs was also performed on a 100-mm-diameter HEMT epiwafer.

## 2.2. Experiment

Samples were grown on 100-mm-diameter and 630-μm-thick *c*-face sapphire substrates using a horizontal MOVPE system (Taiyo Nippon Sanso, SR-4000). Trimethylgallium (TMG), TMA and $NH_3$ were used as Ga, Al and N sources, respectively, and monosilane ($SiH_4$) was used as the n-type dopant. Substrates were first treated in $H_2$ flow at 1180°C, and the temperature was then reduced to 500°C for the growth of 25-nm-thick GaN low-temperature buffer layers (LT-BLs). Subsequently, 3-μm-thick GaN layers and AlGaN layers with thicknesses of 25-200 nm were grown at approximately 1100°C. During the deposition of GaN and AlGaN layers, the flow rates were kept at 20 l/min, 20 l/min, and 40 l/min for $NH_3$ and

its carrier gas, organometallics and their carrier gas, and the top-flow $N_2$ gas, respectively.

The film thickness of the GaN layers was measured by the optical reflectivity method. The thickness of the AlGaN layers was estimated from the growth rate and confirmed by spectroscopic ellipsometry. To confirm the crystal quality of GaN layers and alloy composition of AlGaN layers, X-ray diffraction (XRD) measurement was carried out using a Phillips MRD system. The surface morphology was analyzed using atomic force microscopy (AFM). More detailed information regarding the structural and compositional characterization for epitaxial films is described in Chapter 3. The bowing value of epitaxial wafers was estimated by optical measurement. Hall effect measurement was performed using the Van der Pauw technique to investigate 2DEG properties. Capacitance-voltage (*C-V*) measurements were also carried out to measure the 2DEG density,

HEMTs were fabricated using MOVPE-grown epiwafers, and their device performance was characterized. In order to observe the uniformity of HEMTs DC characteristics, devices were fabricated on a quarter of a 100-mm-diameter AlGaN/GaN epiwafer. The device isolation was accomplished by mesa dry etching down to the GaN layer of HEMT structures by $BCl_3$ plasma reactive ion etching (RIE). The ohmic contact was made by the deposition of Ti/Al/Ni/Au (25/75/20/55 nm), which was subsequently alloyed at 775 °C for 30 s in nitrogen atmosphere using a lamp annealing system. The gate metals of Pd/Ti/Au (40/20/80 nm) were optically defined using conventional photolithography. Electron-beam-evaporated $SiO_2$ films were used for device passivation. Current-voltage (*I-V*) characteristics were measured using a semiconductor parameter analyzer (Agilent 4156c).

## 2.3. Results and discussion

### 2.3.1. Optimization of AlGaN growth on 100-mm-diameter substrates

To investigate the effect of V/III flow ratio on the growth of AlGaN layers, AlGaN layers

were grown at different V/III flow ratios under a constant growth pressure of 100 kPa. In this study, during the deposition of GaN and AlGaN layers, the flow rates were kept at 20 l/min, 20 l/min, and 40 l/min for $NH_3$ and its carrier gas, organometallics and their carrier gas, and the top-flow $N_2$ gas, respectively. Figure 2.1(a) shows Al content in the AlGaN layers and its in-wafer variation as a function of V/III flow ratio with TMA/(TMA + TMG) input gas ratios of 0.2 and 0.25. Here, the V/III flow ratio was controlled by changing the organometallics flow rate with a constant $NH_3$ flow rate of 10 l/min. Al content in the AlGaN layers was estimated using XRD (0004) 2θ-ω scanning, and its in-wafer variation was defined by the expression ((maxim value) – (minimum value))/(mean value) × 100 [%]. More detailed study for the determination of the alloy composition is presented in Chapter 3. Figure 2.1(a) clearly shows that Al incorporation efficiency increased with the increase in the V/III flow ratio. This indicates that the gas phase reaction between TMA and $NH_3$ was reduced by decreasing the organometallics flow rate. Next, AlGaN layers were grown at different growth pressures under constant gas flow conditions with a V/III gas ratio of approximately 10000, and its effect on the AlGaN growth is investigated. Figure 2.1(b) shows the pressure dependence of Al content in the AlGaN layers and its in-wafer variation. It can be seen that compositional uniformity markedly improved by decreasing the growth pressure. It can be speculated that the increased gas velocity that resulted from the decrease in growth pressure suppressed the probability of the molecular collision between TMA and $NH_3$. As a result, the optimized growth conditions of AlGaN layers were obtained, that is, the V/III gas ratio of more than 10000 and the growth pressure of less than 10 kPa. Figure 2.2 shows the solid-vapor composition relationship (Al content x in the AlGaN layers versus TMA/(TMA+TMG) molar fraction) for AlGaN growth. The figure clearly shows a linear relationship, which indicates the preferred incorporation of Al in the AlGaN layers.

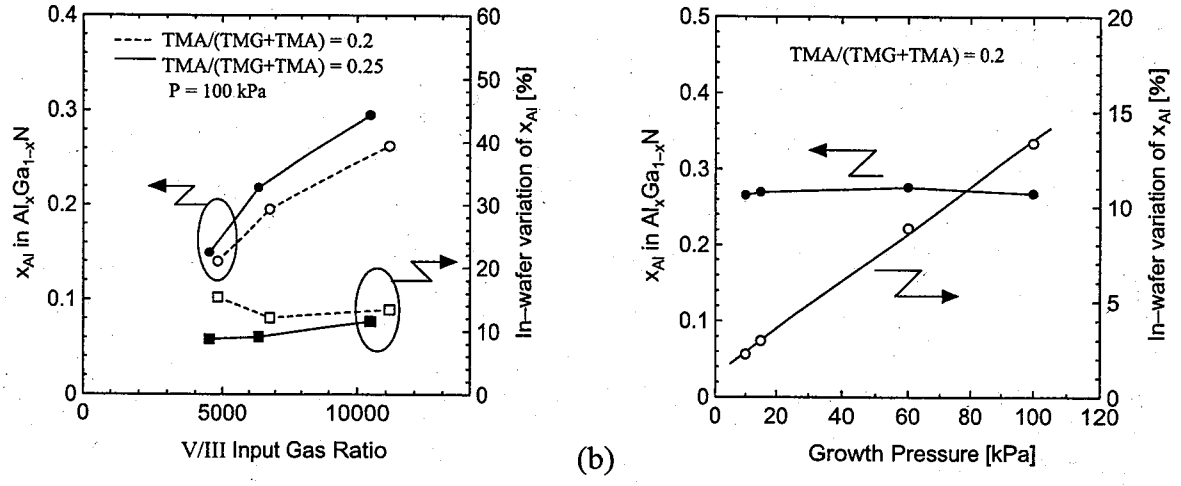


FIG. 2.1. Al content of AlGaN layers and their in-wafer variation as functions of (a) V/III input gas ratio and (b) growth pressure.

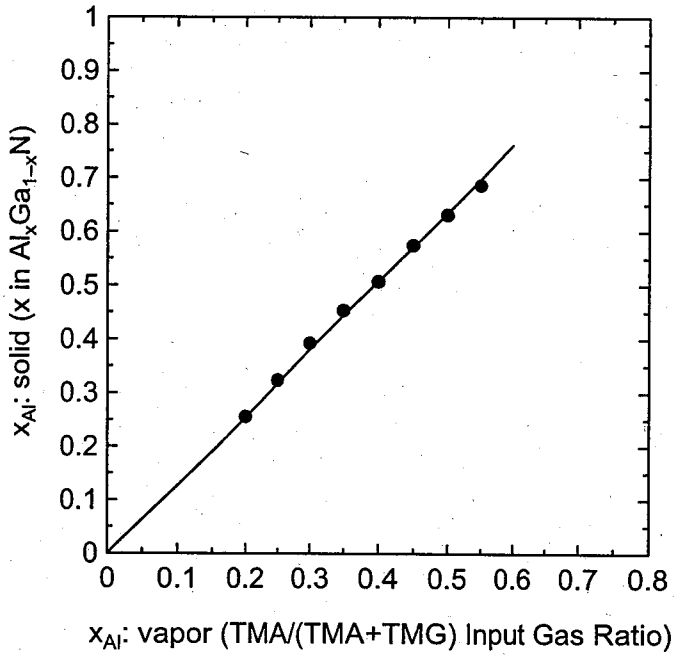


FIG. 2.2. Solid-vapor composition relationship for the growth of AlGaN layers.

### 2.3.2. Structural characterization of MOVPE-grown AlGaN/GaN HEMT wafers

Based on the feasibility study as presented above, we grew different-Al-content AlGaN/GaN HEMT structures on 100-mm-diameter sapphire substrates. Figure 2.3 schematically shows the cross section of present HEMT structures. The present HEMT structure consists of, from top to bottom, a 3-nm-thick nondoped AlGaN layer, a 15-nm-thick silicon-doped AlGaN layer with a doping density of approximately $5 \times 10^{18}/cm^3$, a 7-nm-thick nondoped AlGaN layer, and a 3-μm-thick highly insulating GaN (*i*-GaN) layer. The growth conditions of the *i*-GaN layers have been optimized to obtain a resistivity of higher than $1 \times 10^6$ Ωcm over the entire epitaxial wafer. On the basis of the results shown in Figure 2.2, the Al content $x$ in $Al_xGa_{1-x}N$ layers was designed to be 0.26, 0.33, 0.39, 0.46, 0.52, 0.58, 0.63 and 0.70. Al content in the AlGaN layers and the thicknesses of the GaN and AlGaN layers were confirmed using XRD and spectroscopic ellipsometry, respectively.

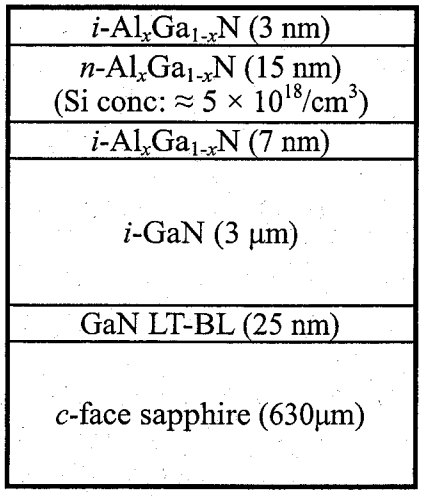


FIG. 2.3. Cross section of MOVPE-grown samples.

Figure 2.4 shows a photograph of a 100-mm-diameter AlGaN/GaN HEMT epiwafer grown using a sapphire substrate. As shown in Figure 2.4, a specular surface was successfully realized across the entire epitaxial wafer, and any irregular surface features such as micro-cracks were not found from observation using Nomarski optical microscope. Figure 2.5 shows the in-wafer thickness uniformity of a GaN layer grown on a 100-mm-diameter sapphire substrate. The thickness variation was as low as ±2% with an average value of 3.04 μm. Figure 2.6 shows the in-wafer distribution of X-ray rocking curve (XRC) full-widths at half maximum (FWHM) for GaN (0004) and (20-24) reflections in a 100-mm-diameter epitaxial wafer. As seen in this figure, XRC FWHM values are relatively small and the in-wafer uniformity is also good. These results indicate that the present 100-mm-diameter GaN layers have good crystal quality and good uniformity over the entire wafer.

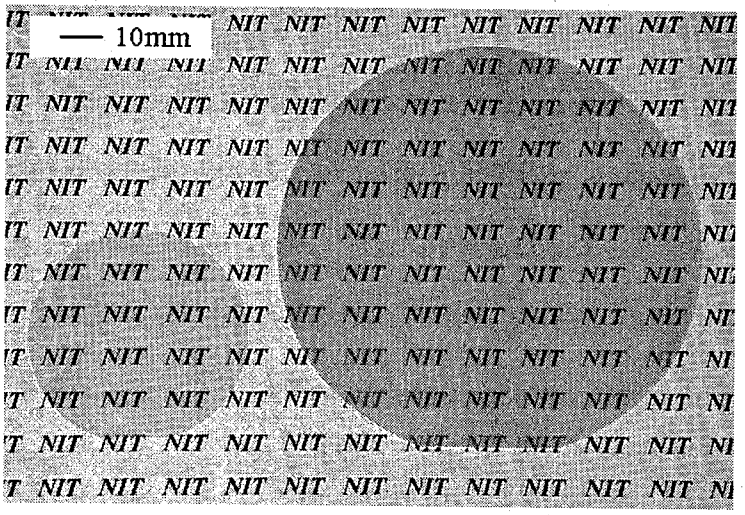


FIG. 2.4. Photograph of 50-mm- and 100-mm-diameter AlGaN/GaN HEMT epiwafers.

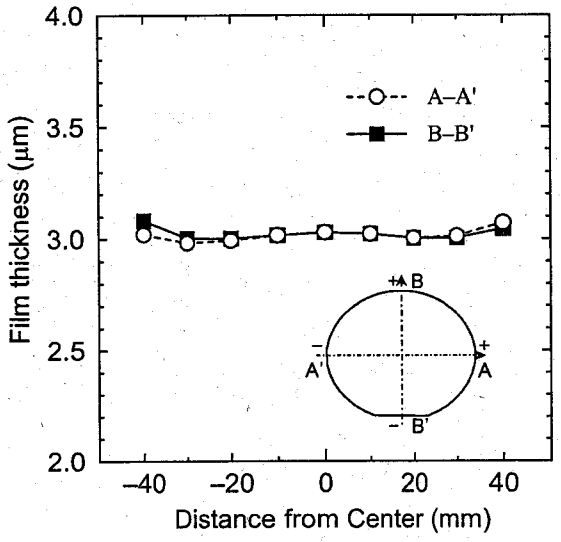


FIG. 2.5. In-wafer thickness variation of a GaN layer grown on a 100-mm-diameter sapphire substrate.

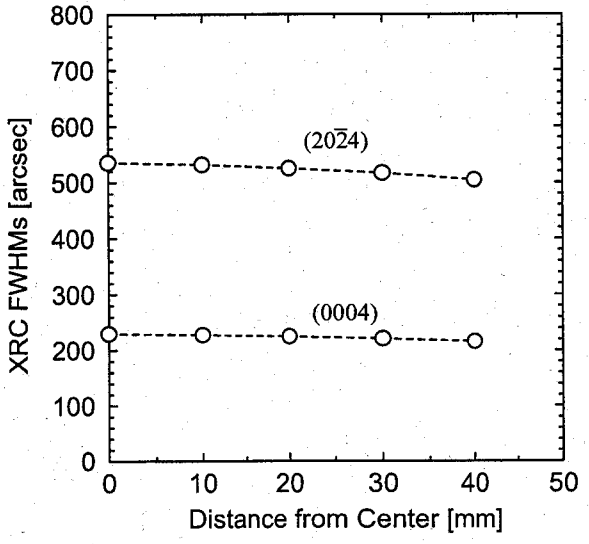


FIG. 2.6. In-wafer distribution of XRC FWHMs for (0004) and (20-24) reflections of a 100-mm-diameter GaN epilayer grown on sapphire.

Figure 2.7 shows the in-wafer uniformity of the AlGaN layer thickness for an $Al_{0.26}Ga_{0.74}N$/GaN HEMT structure grown on a 100-mm-diameter sapphire substrate measured by spectroscopic ellipsometry. The thickness variation was ± 3% with an average value of 25.47 nm. Figure 2.8 shows the in-wafer distribution of the Al content for the different-Al-content AlGaN/GaN HEMT layers. As seen in Figure 2.7, the measured Al contents were in good agreement with the designed values, and good uniformities were also achieved across the entire 100-mm-diameter wafer for all samples. An in-wafer variation of within ± 3.0% was obtained even for the sample with the highest Al content of 0.70.

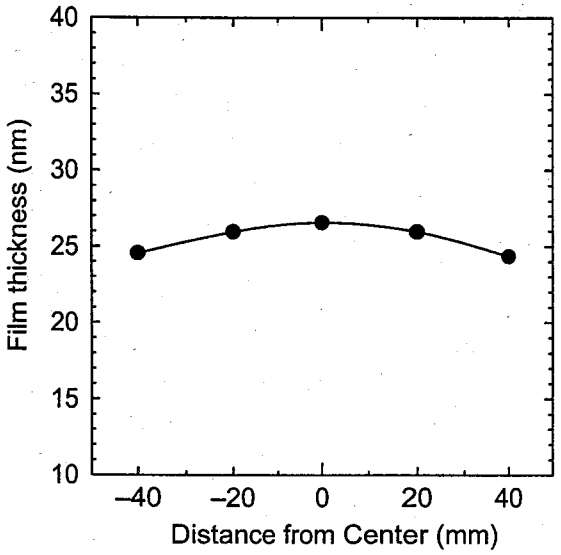


FIG. 2.7. In-wafer thickness variation of an AlGaN layer in a 100-mm-diameter $Al_{0.26}Ga_{0.74}N$/GaN HEMT epiwafer.

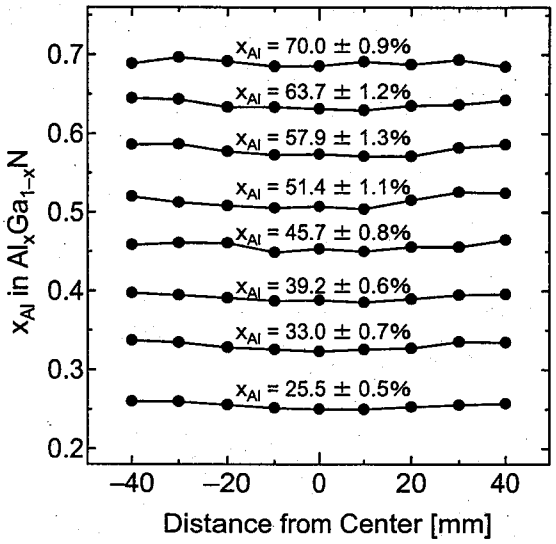


FIG. 2.8. In-wafer distributions of Al contents in different-Al-content AlGaN/GaN HEMT epiwafers.

Figures 2.9(a), 2.9(b), 2.9(c) and 2.9(d) show the AFM images of the different-Al-content $Al_xGa_{1-x}N$/GaN HEMT epilayers ($x$ = 0.26, 0.39, 0.58 and 0.70) for a scanning area of 1 μm × 1 μm. As seen in these figures, the surface exhibited a step-growth-like morphology with some pits for lower-Al-content samples, and a tendency toward an island-growth mode with the increase in Al content in the AlGaN layers. The steps and pits observed in lower-Al-content samples seem to originate from the surface of the underlying GaN layer and from pure edge dislocations, respectively [10,15]. The island-like morphology for higher-Al-content samples seems to be due to the increased stress in the AlGaN layers. As seen in Figure 2.9(d), microcracks were observed on the surface of the sample with Al content of 0.70. We confirmed that microcracks appeared on the samples with the Al content of more than 0.6. This also seems to be due to the increased stress in the AlGaN layers. Figures 2.9(e), 2.9(f), 2.9(g) and 2.9(h) show the XRD reciprocal-space maps (RSM) measured around asymmetric

(20-24) Bragg reflections for the different-Al-content $Al_xGa_{1-x}N$/GaN HEMT layers ($x$ = 0.26, 0.39, 0.58 and 0.70). The XRD RSM figures revealed that the AlGaN layers were coherently grown on the underlying GaN layers for all samples, independent of the existence of microcracks. This is directly evidenced from the fact that the x-coordinates of Bragg reflections from AlGaN layers, which are inversely proportional to the lattice constant of $a$-axis, are almost perfectly aligned with those from the underlying GaN layers. The coherent growth of AlGaN layers is very important for the realization of ideal piezoelectricity at the AlGaN/GaN heterointerface [3].

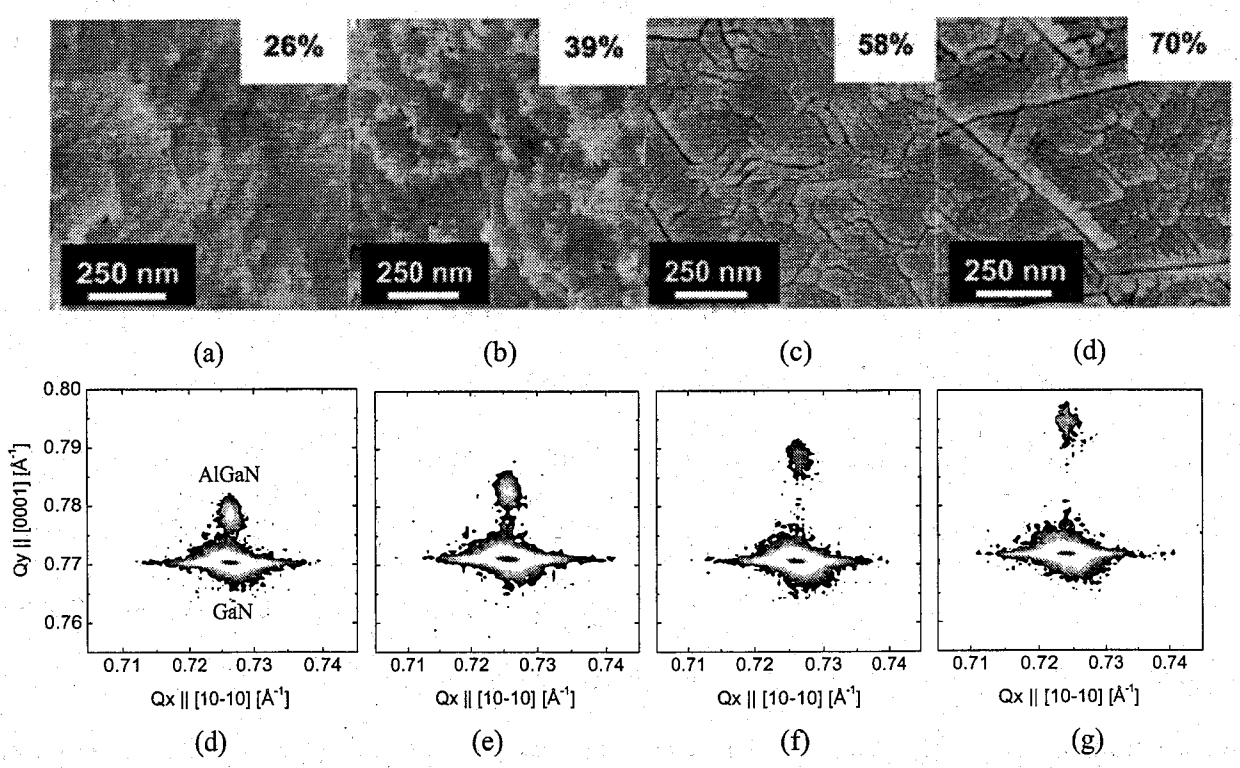


FIG. 2.9. AFM images (scanning area: 1 μm ×1 μm) of MOVPE-grown AlGaN/GaN HEMT layers with Al contents of (a) 0.26, (b) 0.39, (c) 0.58 and (d) 0.70. XRD RSMs taken around (20-24) Bragg reflections of AlGaN/GaN HEMT layers with Al contents of (e) 0.26, (f) 0.39, (g) 0.58 and (h) 0.70. Qx and Qy are the reciprocal lattice vectors in the [0001] and [10-10] directions, respectively, with the units in rlu (1 rlu = $1/d$ Å$^{-1}$, where $d$ represents the lattice spacing).

It is well known that epitaxial growth on large-diameter substrates causes increased bowing of the wafer due to the mismatch in the thermal expansion coefficient and lattice constants between the grown crystals and substrates. For the photolithography process in device production, this is a significant issue that must be solved. Figure 2.10 shows a photograph of optical fringes caused by the bowing of a 100-mm-diameter AlGaN/GaN HEMT epiwafer, which consists of, from top to bottom, a 25-nm-thick $Al_{0.26}Ga_{0.74}N$ layer, a 3-μm-thick GaN layers, a 25-nm-thick GaN LT-BL on a *c*-face sapphire substrate. In Figure 2.10, the fringe spacing corresponds to a vertical interval of 3 μm. From this figure, the bowing value of the epitaxial wafer can be estimated to be approximately 40 μm. This bowing value seems to be sufficiently low to carry out the conventional photolithography process such as that for GaAs-based electronic devices. We also investigated the bowing value of a 100-mm-diameter $Al_{0.26}Ga_{0.74}N$/GaN HEMT structures on *a*-face sapphire substrates by the same method. The obtained bowing value of approximately 100 μm was larger than that on *c*-face sapphire.

Regarding the bowing of GaN epitaxial wafers, Kihara *et al.* reported an experimental and theoretical study using 100-mm-diameter sapphire substrates [16]. In comparison with this previous report, our present results are considered reasonable. The difference in bowing values between the samples grown on *a*- and *c*-face sapphire seems to be caused by the anisotropy of the thermal expansion coefficient in the sapphire crystal. In this study, we used relatively thick (630-μm-thick) sapphire substrates because this thickness seemed to be suitable for conventional device production using, for example, 100-mm-diameter GaAs wafers. We speculate that the relatively low bowing value obtained on *c*-face sapphire is due to the thickness of the sapphire substrates. The previous report also indicated that the bowing value of epitaxial wafers was in proportion to the thickness of epitaxial layers [16]. In the present investigation, add to this, no influence of AlGaN layers on the bowing values of the epitaxial wafers was observed. Hence, lower bowing value could be achieved by reducing the thickness

of GaN layers.

To investigate the relationship between the wafer bowing and the in-plane stress in the films, lattice constants for the GaN layers were estimated using XRD measurements. The measured value of 3.184 Å for *a*-axis was smaller than the intrinsic lattice constants of GaN [17] and almost the same as that for the films on 50-mm-diameter and 330-μm-thick sapphire substrates with the bowing of approximately 30 μm. Judging from these results, the present GaN layers were strained in the direction of in-plane compression, and the stress in the film seems to be almost equivalent to that grown on 50-mm-diameter and 330-μm-thick sapphire substrates. Hence, we can conclude that the reduction of the wafer bowing obtained in this study may not largely increase the in-plane stress in the film.

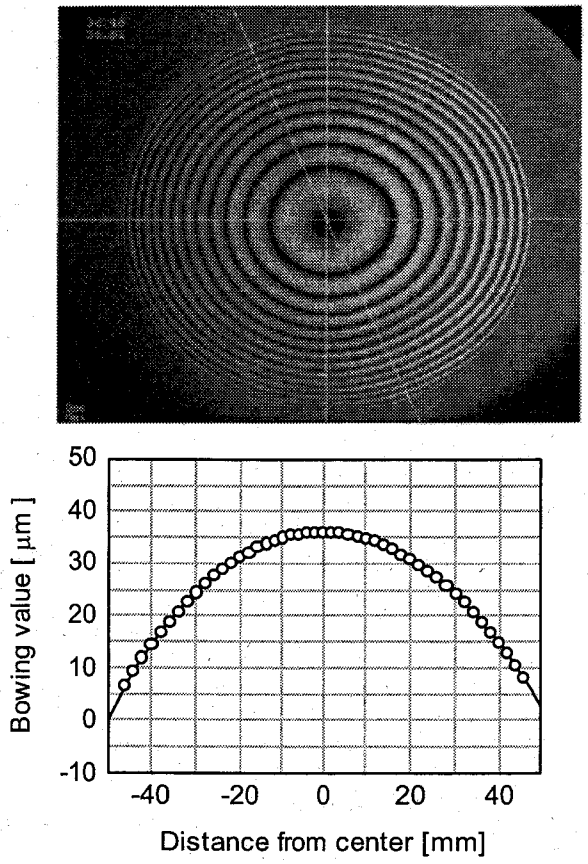


FIG. 2.10. Photograph of fringes caused by the bowing of a 100-mm-diameter AlGaN/GaN HEMT epiwafers , where the distance between fringes corresponds to a vertical interval of 3 μm bowing.

### 2.3.3. Electrical characterization of MOVPE-grown AlGaN/GaN HEMT wafers

Figures 2.11(a), 2.11(b) and 2.11(c) show the in-wafer contour mapping of the sheet resistance for the different-Al-content $Al_xGa_{1-x}N$/GaN HEMT wafers ($x$ = 0.26, 0.39, and 0.52) measured at 81 points in the wafers by the eddy current method. The average sheet resistances were 575 Ω/sq., 438 Ω/sq. and 387 Ω/sq. with total variations of 14.5%, 9.5% and 7.6% and standard deviations of 4.8%, 2.6% and 1.6% for the samples with Al contents of 0.26, 0.39 and 0.52, respectively. Uren *et al.* [18] have reported an average sheet resistance of 695 Ω/sq. with a total variation of 12.3% and a standard deviation of 3.3% for an $Al_{0.24}Ga_{0.76}N$/GaN HEMT layer grown on a 50-mm-diamter sapphire substrate measured by the eddy current method. From this, we understand that the present AlGaN/GaN HEMT wafers have a good electrical uniformity across the 100-mm-diameter epitaxial wafer. Figure 2.11(d) shows the line scan distributions of the sheet resistance ($\rho_s$), electron mobility ($\mu$) and 2DEG density ($n_s$) of the $Al_{0.52}Ga_{0.48}N$/GaN HEMT layer measured by the Hall effect measurement. A high average 2DEG density ($1.76 \times 10^{13}/cm^2$) and a relatively high average electron mobility (971 $cm^2/Vs$) were obtained for the $Al_{0.52}Ga_{0.48}N$/GaN HEMT layer. In addition, the in-wafer uniformity of the 2DEG properties is relatively good. The total variations in the 2DEG density and electron mobility were 7.8% and 8.1%, respectively. Figure 2.11(d) also shows that the sheet resistance measured by the Hall effect (367 Ω/sq.) was almost consistent with that measured by the eddy current method (387 Ω/sq.). Therefore, it can be speculated that the high 2DEG density and relatively high electron mobility were uniformly realized across the 100-mm-diameter epitaxial wafer. We understand that these electrical homogeneities resulted from the structural homogeneities obtained under the optimized growth conditions.

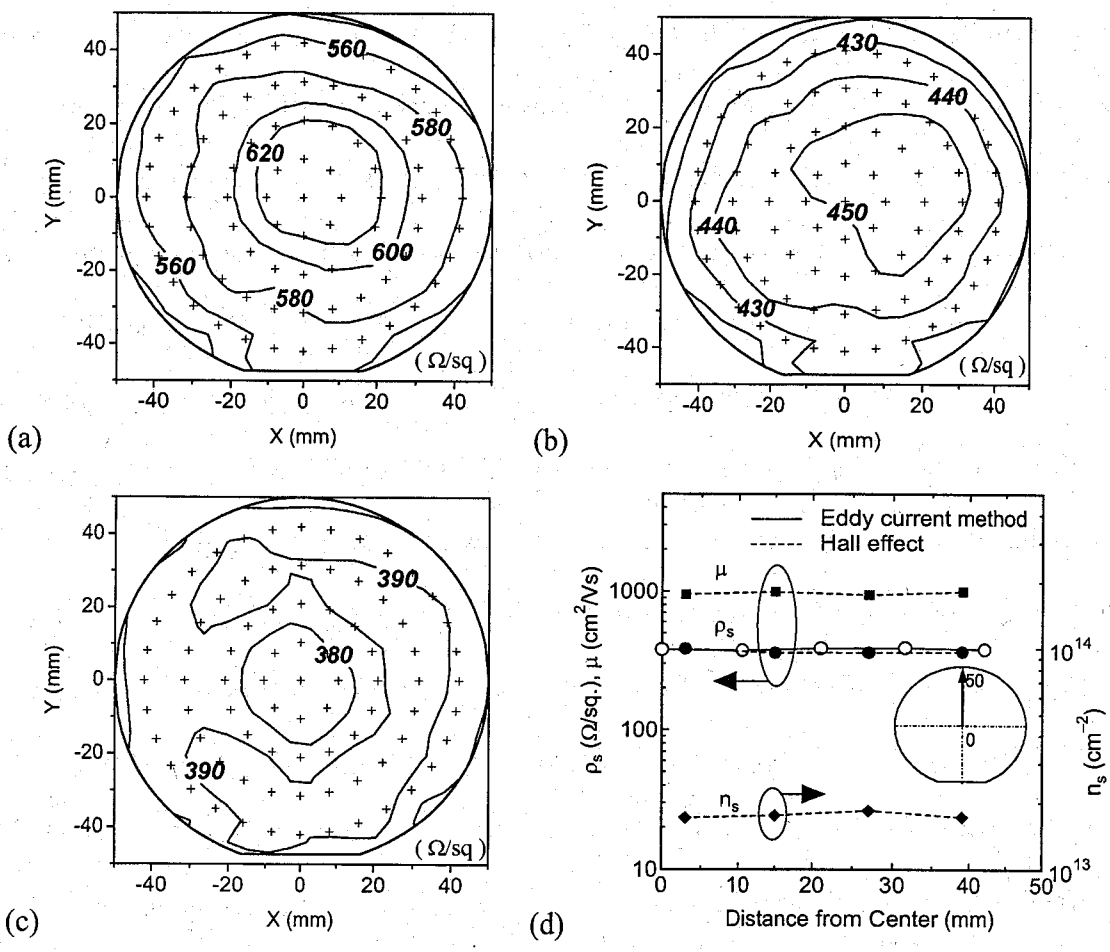


FIG. 2.11. In-wafer sheet resistance mapping of (a) $Al_{0.26}Ga_{0.74}N$/GaN HEMT layer, (b) $Al_{0.39}Ga_{0.61}N$/GaN HEMT layer and (c) $Al_{0.52}Ga_{0.48}N$/GaN HEMT layer measured by the contactless eddy current method. Crosses (+) represent the points of measurement. (d) Line scan distribution of sheet resistance ($\rho_s$), electron mobility ($\mu$) and 2DEG density ($n_s$) across a 100-mm-diameter $Al_{0.52}Ga_{0.48}N$/GaN HEMT wafer measured using the Hall effect measurement (dashed lines) and the eddy current method (solid lines).

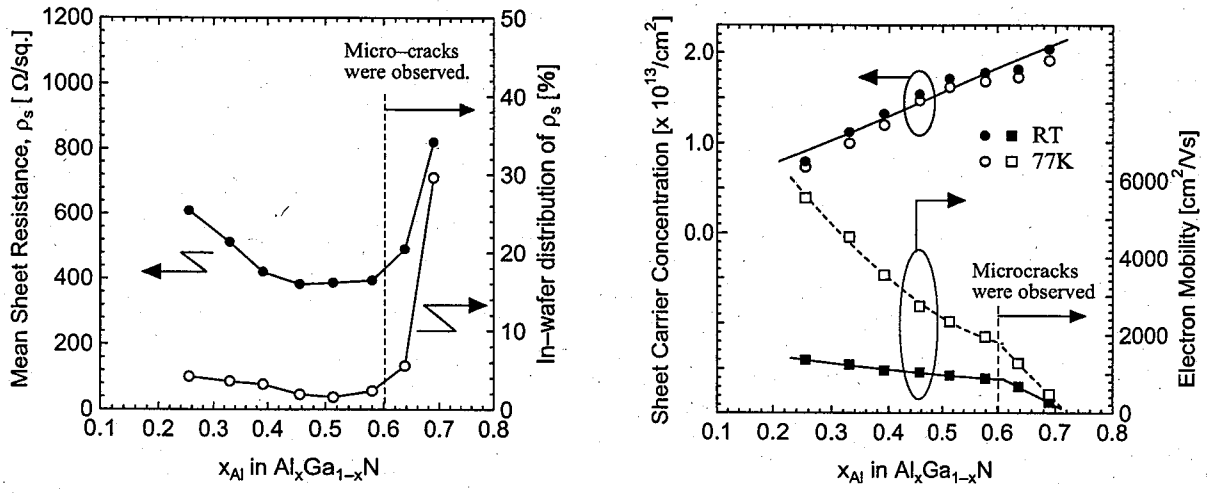


(a) (b)

FIG. 2.12. (a) Sheet resistance and in-wafer distribution of different-Al-content AlGaN/GaN HEMT layers measured by the eddy current method as a function of Al content. (b) 2DEG density and electron mobility of different-Al-content AlGaN/GaN HEMT layers measured using the Hall effect measurement at room temperature and 77 K as a function of Al content.

Figure 2.12(a) shows the mean value and in-wafer distribution of the sheet resistance of the different-Al-content AlGaN/GaN HEMT layers as a function of Al content. These were measured at 81 points in the wafers by the contactless eddy current method. Here, the in-wafer distribution was defined by the expression (standard deviation)/(mean value) × 100 [%]. The in-wafer distribution of the sheet resistance was as low as less than 5.0% for all samples with the Al content up to 0.58. Figure 2.12(a) shows that the sheet resistance decreased with the increase in Al content up to 0.52. For samples with Al contents of 0.63 and 0.70, the sheet resistance and the in-wafer distribution markedly increased. As a result, a minimum sheet resistance of 387 Ω/sq. with an in-wafer distribution of 1.6% was obtained for wafers with the Al content of 0.52. Figure 2.12(b) shows the 2DEG density and electron mobility measured at room temperature (RT) and 77 K as a function of Al content. As seen in Figure 2.12(b), the 2DEG density linearly increased with the increase in Al content, independent of the existence of

microcracks. This result corresponds to the XRD RSM results, that the strain in the AlGaN layers is not relaxed for the underlying GaN layers even for samples with microcracked AlGaN surfaces. Additionally, 2DEG densities measured at RT and 77 K showed approximately the same value, which indicates that 2DEG was well confined at the AlGaN/GaN heterointerface. From Figure 2.12(b), it can also be seen that the electron mobility smoothly decreased with the increase in Al content up to 0.58 and it abruptly decreased for samples with microcracks (Al content x = 0.63 and 0.70). From this, it can be concluded that the increase in the sheet resistance of samples with Al contents of 0.63 and 0.70, as seen in Figure 2.12(a), is due to the decrease in electron mobility caused by the existence of microcracks. On the other hand, electron mobility at room temperature did not significantly decrease with the increase in Al content up to 0.58, as seen in Figure 2.12(b). On the basis of these results, it is concluded that the decrease in sheet resistance with the increase in Al content up to 0.58, as seen in Figure 2.12(a), is due to the increase in 2DEG density. The higher carrier concentration obtained in higher-Al-content HEMT layers presumably results from the increase in the piezoelectric and spontaneous polarization charges at the AlGaN/GaN heterointerface. These 2DEG properties and their compositional dependence are almost comparable to those previously obtained for wafers grown on conventional small substrates [8-10]. Therefore, it is concluded that high-quality AlGaN/GaN HEMT layers with high Al contents of up to 0.58 were uniformly grown on large-area 100-mm-diameter substrates as well as on conventional small substrates. As a result of Hall effect measurement, a minimum sheet resistance of 367 Ω/sq. with a 2DEG density of approximately $1.76 \times 10^{13}/cm^2$ was obtained for the sample with the Al content of 0.52. The further discussions regarding the 2DEG properties obtained in this study are described in Chapter 3 on the basis of the structural characterization results of epiwafers.

## 2.3.4. Fabrication of HEMTs and their characterization results

### 2.3.4.1. DC characteristics in different Al-content AlGaN/GaN HEMTs

HEMTs were successfully fabricated using the present MOVPE-grown epiwafers. Figure 2.13 shows the typical DC $I_{DS}$ – $V_{DS}$ characteristics of the different-Al-content $Al_xGa_{1-x}N$/GaN HEMTs ($x$ = 0.26, 0.39, and 0.52) fabricated using 100-mm-diameter epitaxial wafers, where the gate length and gate width are 2.0 μm and 15.0 μm, respectively. As seen in Figure 2.13, the fabricated devices exhibited good pinch-off characteristics, and it can be observed that the maximum $I_{DS}$ clearly increased with Al content. From Figure 2.13, the decrease in $I_{DS}$ with the increase in $V_{DS}$ for positive gate voltage is observed for all the samples, which is due to the effect of heat generation in the devices [19]. From Figure 2.13, kinks in $I_{DS}$ curves are also observed at a $V_{DS}$ of approximately 7 V in the $Al_{0.52}Ga_{0.48}N$/GaN HEMT. We believe that this is related to the surface degradation of AlGaN layers with increasing Al content (see Figure 2.9).

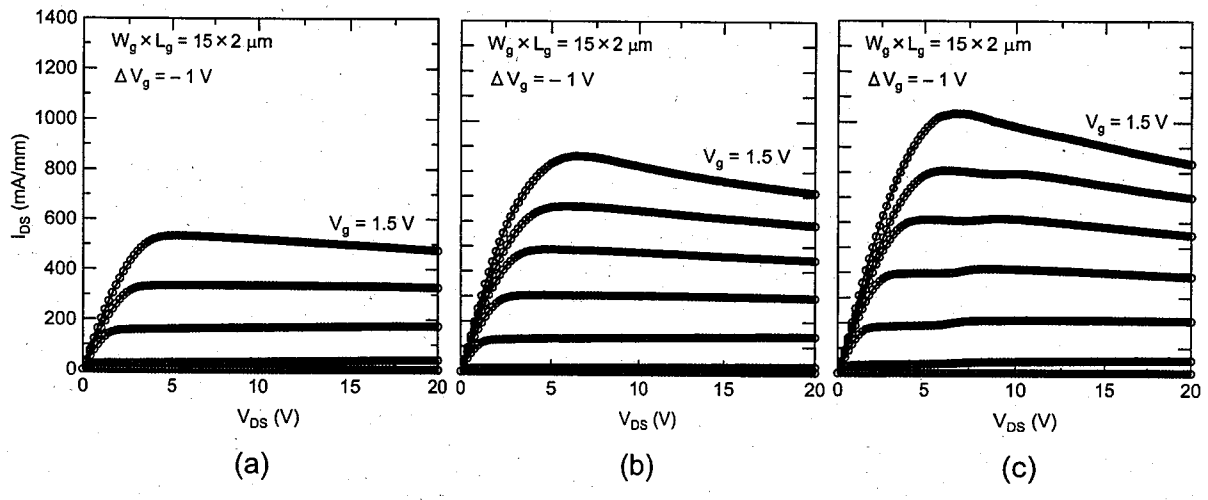


FIG. 2.13. Typical $I_{DS}$-$V_{DS}$ characteristics of (a) $Al_{0.26}Ga_{0.74}N$/GaN HEMTs, (b) $Al_{0.39}Ga_{0.61}N$/GaN HEMTs, and (c) $Al_{0.52}Ga_{0.48}N$/GaN HEMTs ($V_{g,top}$ = + 1.5, $\Delta V_g$ = – 1 V). The device dimensions are $L_{sd}$ = 9 μm, $W_g$ = 15 μm, and $L_g$ = 2 μm.

Figure 2.14 shows the two-terminal gate-leakage current ($I_{GS}$) for the different-Al-content HEMTs. It is clear that $I_{GS}$ increases with Al content. The dependence of $I_{GS}$ on Al content is shown in Table 2.1, where $I_{GS}$ was measured at a $V_{GS}$ of – 40 V. It was found that the $I_{GS}$ of $Al_{0.52}Ga_{0.48}N$/GaN HEMTs was approximately four orders of magnitude higher than that of $Al_{0.26}Ga_{0.74}N$/GaN HEMTs. We understand that the leakage current of a Schottky contact depends on the quality of the interface between the metal and semiconductor. Therefore, it is speculated that the increase in the $I_{GS}$ with Al content is due to the degradation of the surface qualities of AlGaN layers with increasing Al content. In addition, the increase in the root mean square (RMS) surface roughness of AlGaN layers with Al content has also been observed, as shown in Table 2.1. Further investigation is, however, needed regarding the surface degradation of AlGaN layers.

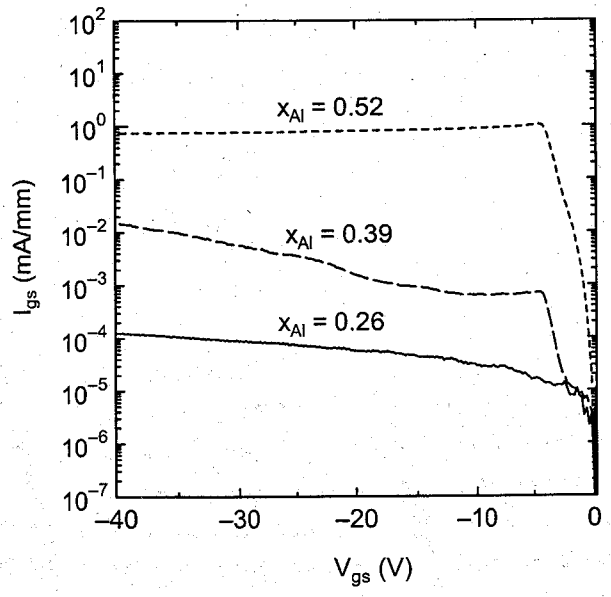


FIG. 2.14. Two terminal gate-leakage current-voltage characteristics of different-Al-content AlGaN/GaN HEMTs.

TABLE 2.1. Average 2DEG densities ($n_S$) and electron mobilities ($\mu$) of MOVPE-grown $Al_xGa_{1-x}N$/GaN HEMT layers ($x$ = 0.26, 0.39, and 0.52) measured by the Hall effect measurement, and DC characteristics ($I_{DS}$max, $g_m$max, $V_{th}$, $R_c$, $R_d$, and $I_{GS}$) in 2.0-μm-gate-length and 15.0-μm-gate-width HEMTs fabricated on different-Al-content $Al_xGa_{1-x}N$/GaN epiwafers ($x$ = 0.26, 0.39, and 0.52). The root mean square (RMS) surface roughness for AlGaN layers measured by AFM (1.0 $\mu m^2$ scan area) is also shown. All the data of HEMT characteristics are typical values of 5-10 devices fabricated on the same wafers.

| $x_{Al}$ (mole fraction) | Hall effect measurement | | HEMT characteristics | | | | | | Surface roughness |
|---|---|---|---|---|---|---|---|---|---|
| | $n_s$ (x $10^{13}$/cm$^2$) | μ (cm$^2$/Vs) | $I_{DS}$ max (mA/mm) | $g_m$ max (mS/mm) | $V_{th}$ (V) | $R_c$ (Ωmm) | $R_d$ (Ωmm) | $I_{GS}$ (A/mm) | RMS (nm) |
| 0.26 | 0.80 | 1360 | 534 | 197 | -2.4 | 2.1 | 5.4 | $1.2 \times 10^{-7}$ | 0.39 |
| 0.39 | 1.32 | 1090 | 862 | 201 | -4.0 | 1.4 | 4.4 | $1.5 \times 10^{-5}$ | 0.47 |
| 0.52 | 1.76 | 971 | 1033 | 228 | -4.2 | 1.9 | 3.9 | $7.5 \times 10^{-4}$ | 0.59 |

The results of maximum $I_{DS}$, maximum $g_m$, threshold voltage ($V_{th}$), contact resistance ($R_c$), drain resistance ($R_d$) and $I_{GS}$ are summarized in Table 2.1. In this table, all the data of HEMT characteristics are typical values of 5-10 devices fabricated on the same wafers. As seen in Table 2.1, the increases in maximum $I_{DS}$ and $V_{th}$ and a reduction in $R_d$ were observed with increasing Al content. These seem to be attributed to the increase in the 2DEG density with Al content. The maximum $I_{DS}$ of $Al_{0.52}Ga_{0.48}N$/GaN HEMTs was approximately twofold that of $Al_{0.26}Ga_{0.74}N$/GaN HEMTs. This corresponds to the result that the 2DEG density of $Al_{0.52}Ga_{0.48}N$/GaN HEMT layers was approximately twofold that of $Al_{0.26}Ga_{0.74}N$/GaN HEMT layers. The highest $I_{DS}$ of 1033 mA/mm with a maximum $g_m$ of 228 mS/mm was observed for $Al_{0.52}Ga_{0.48}N$/GaN HEMTs. We have also confirmed that the uniformity of HEMTs DC properties is in good correlation with the electrical characteristics of AlGaN/GaN HEMT wafers obtained by the Hall effect measurement (see section 2.3.4.2). From this, it can be speculated that the high $I_{DS}$ and $g_m$ values are uniformly realized across the entire 100-mm-diameter wafer. The contact resistances of the present devices are, however, relatively high compared with the previously reported values [11,12]. We believe that further improvements in ohmic contact formation contribute to the fabrication of high-performance HEMTs.

### 2.3.4.2. Uniformity study of AlGaN/GaN HEMTs grown on 100-mm-diameter sapphire

A quarter of a 100-mm-diameter $Al_{0.26}Ga_{0.74}N$/GaN epiwafer was used for the uniformity study of HEMTs. The isolation current was measured at 40 different locations on a quarter of the 100-mm-diameter wafer. Except the periphery of the wafer, the isolation current of *i*-GaN varies between 0.17 nA to 0.5 μA. The DC characteristics of the fabricated HEMTs were measured using semiconductor parameter analyser. Identical device dimensions ($W_g$=15 μm, $L_g$=2.0 μm, $L_{SG}$=2.0 μm, $L_{SD}$=9.0 μm) were chosen for the uniformity studies across the wafer. Figures 2.15(a), 2.15(b) and 2.15(c) show the contour mapping of $I_{DS}$max and $g_m$max and threshold voltage ($V_{th}$) of AlGaN/GaN HEMTs on a quarter of the 100-mm-diameter substrate. The average $g_m$max and $I_{DS}$max values of 197 mS/mm and 515 mA/mm with standard deviations of 4.82% and 9.34% respectively were observed on a quarter of the 100-mm-diameter wafer. The uniformity of the devices are in agreement with the uniformity of Hall mobility and 2DEG density of 1322 $cm^2$/Vs and 8.36 × $10^{12}$/$cm^2$ with standard deviations of 4.27% and 6.75%, respectively. Generally, 2DEG density in AlGaN/GaN structures depends on both the AlGaN doping concentration and AlGaN layer thickness. In this case, we believe that the AlGaN thickness is a more dominant cause for the variation of the 2DEG density when compared with the AlGaN doping concentration. The average values of source ($R_s$) and drain ($R_d$) resistance are 2.64 ±0.20 Ω-mm and 5.80 ±0.37Ω-mm, respectively. It is clear that both the $R_s$ and $R_d$ variations are less than 7.5%. The average $V_{th}$ values of the devices are -2.30 V with a standard deviation of 6.52% (see Figure 2.15(d)). The *C-V* measured average $V_{th}$ values (-2.33 V with a standard deviation of 6.65%) are in good agreement with the values obtained from $\sqrt{I_D} - V_G$ plot of HEMTs. From this, it is clear that, the AlGaN/GaN HEMTs on the 100-mm-diameter sapphire substrate were in good homogeneity across the wafer.

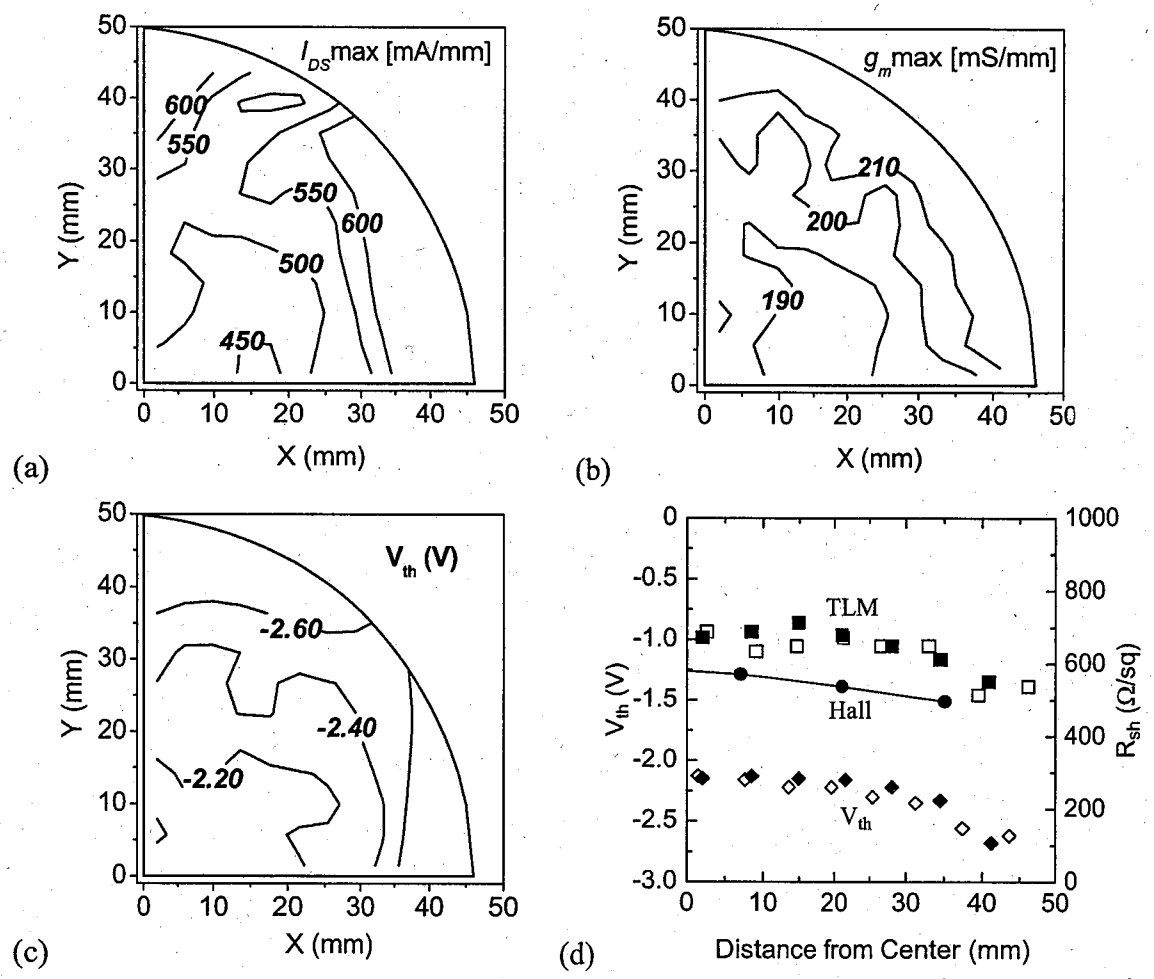


FIG. 2.15. Contour mapping of a) $I_{DS}$max, b) $g_m$max and c) $V_{th}$ of AlGaN/GaN HEMTs on a quarter of 100-mm-diameter wafer. d) Line scan distribution of $V_{th}$ and sheet resistance measured from Hall and TLM method. Open and filled symbols denote the X- and Y-axis distribution of a quarter of the 100-mm-diameter wafer.

To measure the 2DEG density, *C-V* measurements were carried out at 1 MHz on 40 identical diameter Schottky diodes at different locations of a quarter of the 100-mm-diameter wafer using HP4845A LCR meter. The average peak 2DEG density measured from *C-V* measurements is $3.69 \times 10^{19}/cm^3$ at a depth of $22.51 \pm 1.78$ nm. The carrier density at a depth above 2 μm was as lows as $5 \times 10^{12}/cm^3$. The combination of low leakage current of *i*-GaN and the observation of minimum carrier density at a depth of 2 μm indicate that the present MOVPE-grown AlGaN/GaN heterostructures have good quality with highly-insulating GaN layer across the entire 100-mm-diameter wafer.

## 2.4. Conclusion

The growth conditions of AlGaN layers were optimized using a large-size MOVPE system, and different-Al-content AlGaN/GaN HEMT structures with the highest Al content of 70 mol% were successfully grown on 100-mm-diameter sapphire substrates. It was confirmed that all of the present HEMT layers showed specular surface morphology and have a good in-wafer uniformity of the layer structures and film qualities. It was also confirmed that no relaxation in the AlGaN layers occurred for any of the samples. The results of electrical characterization revealed a high homogeneity of MOVPE-grown AlGaN/GaN HEMT layers except when microcracks appeared on the AlGaN surface. A minimum sheet resistance of approximately 380 Ω/sq (2DEG density = $1.76 \times 10^{13}/cm^2$) with good in-wafer uniformity was obtained for the sample with the Al content of 52 mol%.

The bowing value of the 100-mm-diameter AlGaN/GaN HEMT wafers was approximately 40 μm in the case of samples grown on *c*-face sapphire. This bowing value seems to be preferable for electronic device fabrication processes. HEMTs were successfully fabricated and they exhibited good pinch-off properties. The dependence of $I_{DS}$ on Al content was consistent with the Al-content dependence of 2DEG density. The maximum source-drain

current density of 1033 mA/mm with a maximum extrinsic transconductance of 228 mS/mm was obtained for 2-μm-gate-length $Al_{0.52}Ga_{0.48}N$/GaN HEMTs.

To observe the uniformity of HEMTs DC characteristics, devices were fabricated at 40 locations on a quarter of 100-mm-diameter $Al_{0.26}Ga_{0.74}N$/GaN heterostructures. The observed average $I_{DS}$ max, $g_m$max and $V_{th}$ values for HEMTs were 515 mA/mm, 197 mS/mm and -2.30 V with standard deviations 9.34%, 4.82% and 6.52%, respectively. The standard deviation of $g_m$max is in good agreement with the uniformity of 2DEG properties across the 100-mm-diameter wafer. The Hall effect and TLM measured sheet resistance of the AlGaN/GaN heterostructures were in good uniformity with the standard deviations of 9.01% and 9.43%, respectively. The uniformity of HEMTs DC characteristics were in good correlation with the electrical characteristics of AlGaN/GaN heterostructures, which was obtained from the Hall Effect and *C-V* measurements. In conclusion, the present MOVPE-grown 100-mm-diameter epiwafers are suitable for the mass production of high power/microwave device applications and fabrications.

## References


[1] D. Bykhovski, B. L. Gelmont, and M. S. Shur, J. Appl. Phys. **81**, 6332 (1997).

[2] E. T. Yu, G. J. Sullivan, P. M. Asbeck, C. D. Wang, D. Qiao, and S. S. Lau, Appl. Phys. Lett. **71**, 2794 (1997).

[3] T. Takeuchi, H. Takeuchi, S. Sota, H. Sakai, H. Amano, and I. Akasaki, Jpn. J. Appl. Phys. **36**, L177 (1997).

[4] O. Ambacher, J. Smart, J. R. Shealy, N. G. Weimann, K. Chu, M. Murpjy, W. J. Schaff, L. F. Eastman, R. Dimitrov, L. Wittmer, M. Stutzmann, W. Rieger, and J. Hilsenbeck, J. Appl.

Phys. **85**, 3222 (1999).

[5] F. Bernardini and V. Fiorentini, Phys. Rev. **B 56**, R10024 (1997).

[6] Y. Zhang, I. P. Smorchkowa, C. R. Elsass, S. Keller, J. P. Ibbetson, S. DenBaars, U. K. Mishra, and J. Singh, J. Appl. Phys. **87**, 7981 (2000).

[7] N. Maeda, T. Nishida, N. Kobayashi, and M. Tomizawa, Appl. Phys. Lett. **73**, 1856 (1998).

[8] P. Smorchkova, C. R. Elsass, J. P. Ibbetson, R. Vetury, B. Heying, P. Fini, E. Haus, S. P. DenBaars, J. S. Speck, and U. K. Mishra, J. Appl. Phys. **86**, 4520 (1999).

[9] P. M. Asbeck, E. T. Yu, S. S. Lau, G. J. Sullivan, J. Van Hove and J. Redwing, Electron. Lett. **33**, 1230 (1997).

[10] S. Keller, G. Parish, P. T. Fini, S. Heikman, C.-H. Chen, N. Zhang, S. P. DenBaars, U. K. Mishra, and Y.-F. Wu, J. Appl. Phys. **86**, 5850 (1999).

[11] U. K. Mishra and Y. -F. Wu, IEEE Trans. Microwave Theory Tech. **46**, 756 (1998).

[12] Y.-F. Wu, B. P. Keller, P. Fini, S. Keller, T. J. Jenkins, L. T. Kehias, S. P. Denbaars and U. K. Mishra, IEEE Electron Device Lett. **19**, 50 (1998).

[13] C. H. Chen, H. Liu, D. Steigerwald, W. Imler, C. F. Kuo, and M. G. Craford, *Mat. Res. Soc. Proc.*, **395**, 103 (1996).

[14] K. Nakamura, O. Makino, A. Tachibana, and K. Matsumoto, J. Organomet. Chem., **611**, 514 (2000).

[15] X. H. Wu, L. M. Brown, D. Kapolnek, S. Keller, B. Keller, S. P. DenBaars, and J. S. Speck, J. Appl. Phys. **80**, 3228 (1996).

[16] M. Kihara, T. Sasaki, T. Tsuchiya, and H. Sakaguchi, *Proc. Int. Workshop on Nitride Semiconductors (IWN)*, IPAP Conf. Series 1, 117 (2000).

[17] T. Detchprohm, K Hiramatsu, K Itoh, and I. Akasaki, Jpn. J. Appl. Phys. **31**, 1154, (1992).

[18] M. J. Uren, D. Leea, B. T. Hughes, P. J. M. Parmiter, J. C. Birbeck, R. Balmer, T. Martin,

R. H. Wallis, and S.K. Jones, J. Cryst. Growth **230**, 579 (2001).

[19] R. Gaska, A. Osinky, J. W. Yang, and M. S. Shur, IEEE Electron Device Lett. **19**, 89 (1998).